A Continuous-Time Model with Monte Carlo Simulation for Smartphone Battery Time-to-Empty Prediction and Optimization

Assessing the endurance of smartphone lithium-ion batteries remains a critical challenge, hindered by dynamic usage patterns, environmental fluctuations, and electrochemical complexities. Traditional empirical models often fail to capture the coupled effects of multi-component power consumption and battery aging, leading to unreliable time-to-empty (TTE) predictions. To address this gap, we proposed a white-box, physics-driven framework that integrates a continuous-time battery model with stochastic scenario analysis. This approach uses coupled ordinary differential equations to describe state-of-charge dynamics, polarization voltage, temperature evolution, and capacity fade, achieving validation accuracy of less than 5% against public datasets.

Firstly, for the continuous-time battery modeling component, we derived a system of coupled ordinary differential equations that capture the core electro-thermal dynamics of lithium-ion batteries.It incorporates SOC kinetics rooted in energy conservation, polarization dynamics via RC network analogs, and thermal behavior through heat transfer equations.Solved using fourth-order Runge-Kutta methods, the model exhibits exceptional robustness across diverse operating conditions, with high precision in capturing voltage sag under high-current loads. Validation against experimental data confirms voltage-SOC relationship errors of less than 5%, outperforming empirical alternatives by explicitly accounting for aging effects.

Secondly, to quantify TTE under stochastic user behavior,we extended the model with Monte Carlo simulations incorporating usage pattern stochasticity and implemented a Continuous-Time Markov Chain (CTMC) approach to model transitions between power states.Drawing on 1000 simulations, we generated probabilistic TTE distributions that reflect real-world uncertainty-a capability absent in most existing models.

Thirdly,through Sobol-index-based global sensitivity analysis, the model maintained predictive accuracy despite parameter uncertainties. The analysis identified capacity (67%) and internal resistance (18%) as the principal contributors to output variance, with remaining parameters collectively accounting for the residual 15%. Meanwhile, parameter perturbation experiments with ±20% variations demonstrated the model's stability.Furthermore, the framework accurately predicts real-world phenomena like sudden shutdowns triggered by voltage cutoff thresholds, demonstrating its practical utility.

Practical applications include user-centric strategies and operating system-level optimizations. Notably, reducing screen brightness emerges as the most impactful user-level intervention, potentially extending TTE by 15~20% due to the display's dominant 40~50% share of total power consumption. For system-level implementation, we proposed dynamic power management algorithms that adjust CPU frequencies and network usage based on real-time SOC and temperature. Critically, the framework generalizes seamlessly to other portable devices–including laptops and wearables-via parameter recalibration, delivering consistent performance across platforms and highlighting its scalability.

Keywords: lithium-ion battery, continuous-time model, Monte Carlo simulation, sensitivity analysis, energy optimization

Contents

1 Introduction

1.1 Problem Background

Smartphone lithium ion battery performance usually exhibits significant variability due to multifaceted factors beyond usage intensity, revealing the limitations of simplistic monitoring approaches in capturing the electrochemical complexities of lithium-ion batteries. Battery behavior is governed by three interconnected factors: user-specific patterns, hardware-dependent characteristics, and persistent background activities. Environmental conditions, particularly temperature, play a critical role-cold environments reduce capacity and increase internal resistance, while high-load operation causes overheating and accelerates aging. These temperature-dependent dynamics create nonlinear couplings between operating conditions and battery lifespan, necessitating dynamic electro-thermal coupled models for accurate performance prediction.

1.2 Restatement of the Problem

Based on the identified challenges, we formalized the core research problems. Our modeling approach was designed to systematically address these questions in a continuous-time framework.

- **Problem 1 (Model Formulation):** Develop a continuous-time differential equation model to describe the dynamics of battery state of charge (SOC).
- **Problem 2 (Prediction & Validation):** Predict Time-To-Empty (TTE) under diverse initial SOC levels and usage scenarios, validating the model against observed behavior and quantifying predictive uncertainty.
- **Problem 3 (Robustness Analysis):** Assess model robustness via sensitivity analysis of key assumptions, parameters, and usage pattern fluctuations.
- **Problem 4 (Application & Extension):** Formulate practical power management recommendations for users and operating systems, and evaluate the model's generalizability to other portable devices.

1.3 Literature Review

A significant gap persisted in the literature: most studies focused either on electrochemical principles or on empirical usage patterns, but few offered a unified modeling framework that integrates internal battery dynamics with external, stochastic user behavior.

- Lithium-ion battery performance degrades through mechanisms such as capacity fade, increased internal resistance, voltage anomalies, and lithium plating. These failures collectively reduce performance, reliability, and safety [1].
- Empirical studies, such as examining NCM pouch-type batteries, confirmed that operational temperature is a critical variable, directly impacting capacity and heat generation [2].
- While simple continuous-time models like Enhanced Coulomb Counting exist, they often fail under real-world conditions. Their primary weakness is an inability to adequately incorporate nonlinear factors, such as the dynamic interplay between internal resistance, temperature, and capacity-a core requirement of this problem [3].
- Predictive methods like deterministic scenario simulation and local sensitivity analysis are common but limited. The former assumes constant usage patterns, an unrealistic idealization, while the latter cannot analyze the interactions between multiple, co-varying factors that affect battery drain [4].

The advantages and disadvantages of three conservational approaches are summarized in Figure 1.
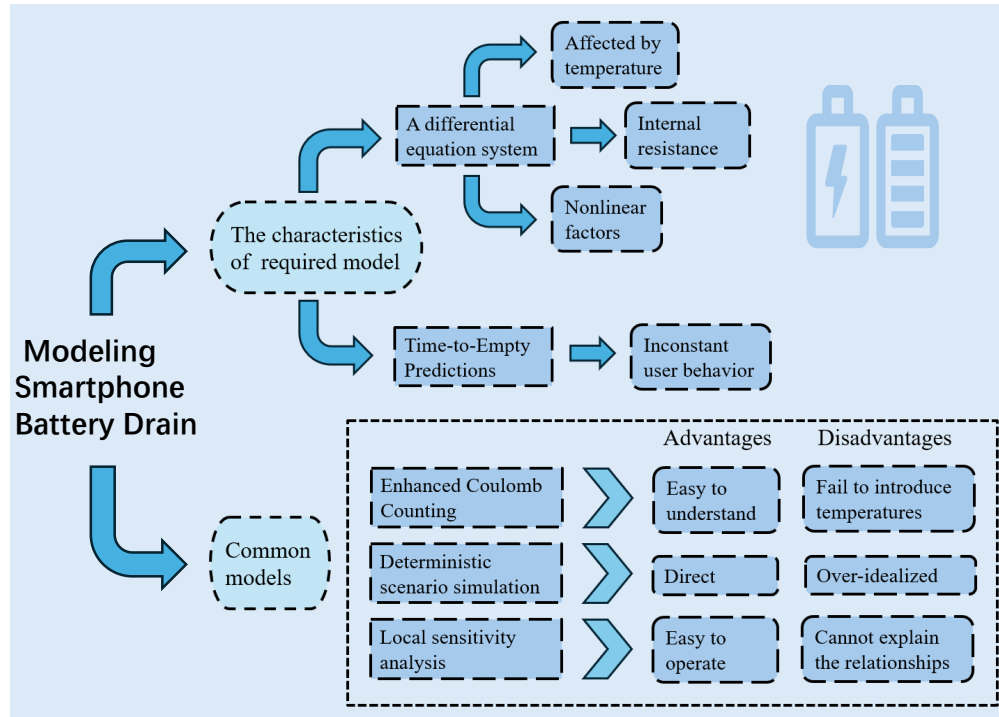
Figure 1: Literature Review

1.4   Our work

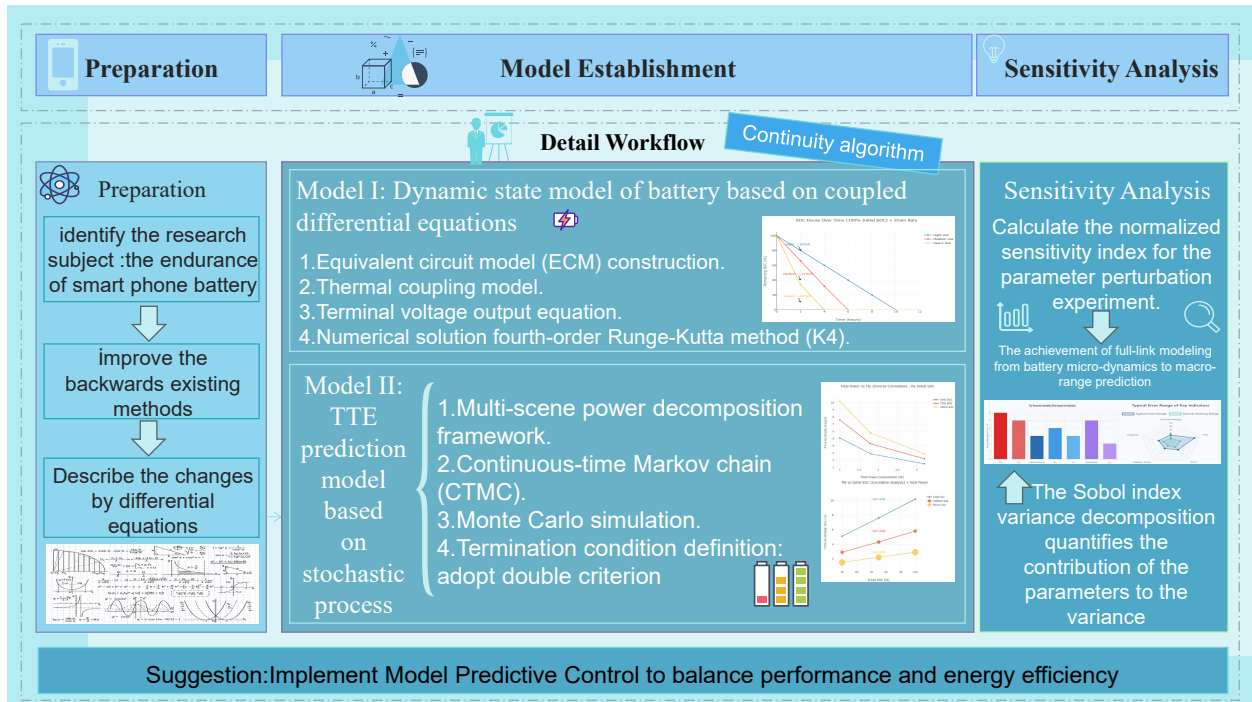In order to clearly illustrate our work, we drew the flowchart Figure 2.

Figure 2: Our work

Our work addressed this gap by developing a comprehensive electro-thermal model that bridges this divide, capturing the continuous-time interaction between battery physics and real-world operational conditions.

2 Model Preparing

2.1 Assumptions and Justifications

The following reasonable assumptions can be made in this paper:

- **Assumption:** The dynamics of battery state evolution can be accurately described by a system of differential equations.
- **Justification:** Differential equations provide a natural mathematical framework for modeling continuous-time processes governed by physical laws, such as energy conservation, fulfilling the problem's requirement for a mechanistic and time-continuous formulation.
- **Assumption:** Within typical operating temperatures (e.g., 10~25°C), the internal resistance and effective capacity of the battery vary linearly with temperature.
- **Justification:** Within a limited temperature range, the use of the linear approximation method can achieve an effective balance between model accuracy and parameter simplicity, making it suitable for short-term predictions.
- **Assumption:** During idle periods, background applications sustain a consistent power draw unless altered by explicit user intervention.
- **Justification:** This reflects real-device behavior where processes such as push notifications and system services maintain a low-level steady-state energy consumption.
- **Assumption:** Battery aging effects are negligible in short-term simulations (e.g., $\leqslant$ 1 day) but adhere to an exponential decay model over extended periods.
- **Justification:** Ignoring the capacity decline that occurs only after multiple charging cycles in daily simulations does not significantly affect the accuracy. However, using an exponential decay form ensures the model's scalability in long-term analysis.

2.2 Notations

The key mathematical notations used in this paper are listed in Table 1.

Table 1: Notations

Symbol	Unit	Definition
Q_{ref}	mAh	Typical capacity of modern flagship smartphones
Q_{eff}	mAh	The effective available capacity of the battery
V_{nom}	V	Standard operating voltage platform for lithium-ion batteries
V_{min}	V	Voltage at which the protection circuit cuts off the power
V_{max}	V	Voltage at 100% State of Charge
R_{int}	Ω	Internal resistance, increases sharply with decreasing temperature
m_{bat}	kg	Battery mass, used for thermal capacity calculation
C_p	J/(kg·K)	Average specific heat capacity of lithium-ion battery materials
h_{eff}	W/K	Effective heat transfer coefficient representing heat dissipation capability
η	-	Coulombic efficiency, decreases with aging or at low temperatures

There are some variables that are not listed here and will be discussed in detail in each section.

2.3 Data Collecting and Processing

To fulfill the problem's requirement of developing a physically consistent continuous-time model, our approach prioritizes data for "parameter estimation and validation", not as a substitute for mechanistic reasoning. All data utilized are from well-documented, openly licensed sources, ensuring reproducibility and transparency. This section details our data collection strategy and processing pipeline, which is designed to bridge the gap between device-level power consumption and fundamental battery electrochemistry.

2.3.1 Data Sources and Rationale

Our modeling framework necessitated two primary categories of data, meticulously selected to satisfy the problem's dual focus on usage patterns and battery physics.

Source A: The AndroWatts Dataset (Zenodo): This dataset is instrumental in defining realistic, time-varying load currents $I(t)$ for our differential equations, directly addressing the problem's emphasis on factors like screen usage, processor load, and network connections.

- provides aggregated metrics from 1,000 stimulation tests on mobile devices.
- captures the dynamic interplay between device state variables (e.g., screen brightness, network activity, temperature, SOC, CPU/GPU frequency) and the power consumption of individual hardware components.
- source:https://zenodo.org/records/14314943
- DOI:10.5281/zenodo.14314943
- license:CC BY 4.0 (Creative Commons Attribution 4.0)

Source B: The Battery Degradation Datasets (Mendeley Data): This directly supports the problem's requirement to consider how "battery aging reduces effective capacity".

- contains cycling data for two distinct lithium-ion battery types.
- provides the empirical foundation for extracting the Open-Circuit Voltage (OCV) vs. State of Charge (SOC) relationship, V_{ocv}(SOC), and for analyzing the effects of aging (State of Health, SOH) on effective capacity Q_{eff} and internal resistance.
- source:https://data.mendeley.com/datasets/v8k6bsr6tf/1
- DOI:10.17632/v8k6bsr6tf.1
- license:CC BY 4.0

2.3.2 Data Preprocessing and Feature Engineering

A rigorous preprocessing pipeline was implemented to transform raw data into features compatible with our electro-thermal model.

AndroWatts Data Processing: The core file was processed as follows:

- **Unit Standardization:** Critical measurements were converted to standard scientific units (e.g., temperature from milliCelsius to Celsius, battery percentage to a fractional SOC).
- **Load Current Derivation:** The discharge current $I(t)$ was calculated from the provided battery discharge rate, serving as a direct input to the SOC state equation.
- **Total Power Calculation:** Power consumption from all individual components (display, CPU, WiFi, etc.) was summed to obtain the total system power draw, P_{total}.

Battery Electrochemical Data Processing: Data from the Excel files were processed to extract key battery parameters:

- **Capacity and SOH Calculation:** For each charge-discharge cycle, the maximum capacity

Q_{full} was identified. The State of Health (SOH) was calculated as the ratio of the current cycle's capacity to the initial capacity.

- **Representative Aging States:** Six representative SOH levels were selected (from "New" to "End-of-Life") to model the impact of battery degradation over time.
- **OCV-SOC Relationship Fitting:** For each representative battery state, the voltage-capacity data from the constant-current charging phase was used to fit a fifth-order polynomial, $V_{ocv}(\text{SOC}) = \sum_{i=0}^{5} c_i \text{SOC}^i$, yielding the coefficients used in terminal voltage equation (5).

2.4   Defining Specic Usage Scenarios

2.4.1   Rationale and Methodology for Scenario Definition

To derive realistic Time-to-Empty (TTE) predictions, we defined a set of characteristic usage scenarios grounded in data from the AndroWatts dataset and established literature. Our methodology employed k-means clustering on key power metrics-screen, CPU, network, GPS, background processes, and total system power-to identify distinct behavioral patterns. For each cluster, we extracted representative parameters for all power-consuming components and validated the resulting scenarios against published power profiling studies to ensure physical consistency. This data-driven approach ensured our scenarios are both empirically grounded and representative of real user behavior.

Five scenarios were defined, ordered by increasing power demand:

- Standby Mode (screen off, minimal background activity);
- Web Browsing (moderate screen brightness, periodic network requests, medium CPU);
- Video Streaming (high brightness, continuous playback, display-dominated load);
- Gaming (maximum CPU/GPU, high brightness, intensive 3D rendering);
- Navigation (continuous GPS, moderate screen and CPU usage)

Table 2 provides the detailed power decomposition for each scenario under standard conditions (200 nits, 25°C).

Table 2: Power consumption decomposition for characteristic usage scenarios (units: Watts)

Scenario	Display	CPU/GPU	Network	GPS	Background	Total
Standby	0.00	0.05	0.02	0.00	0.08	0.15
Web Browsing	0.36	0.23	0.15	0.00	0.10	0.84
Video Streaming	0.64	0.50	0.25	0.00	0.10	1.49
Gaming	1.00	1.35	0.15	0.00	0.10	2.60
Navigation	0.49	0.30	0.35	0.30	0.10	1.54

2.4.2   Scenario Integration with Battery Model

These scenario definitions translate discrete usage patterns into specific power consumption profiles $P_{\text{total}}(s, t)$ (where s denotes the scenario type), which serve as direct input to our coupled ODE system. This approach enables the modeling of realistic, non-uniform workloads and facilitates several critical analyses. It allows for systematic comparative analysis of battery performance across activities and sensitivity analysis to isolate the impact of individual components (e.g., screen

vs. CPU). Furthermore, the framework provides a foundation for personalized predictions by accommodating user-specific habit profiles.

In simulations, each scenario is implemented with constant power characteristics for simplicity, though the model structure supports time-varying $P_{\text{total}}(t)$ for advanced studies. This methodology effectively bridges component-level power data with the electrochemical battery model, enabling realistic, scenario-specific predictions that meet the problem's requirement for multi-condition analysis.

3   Model I : A differential equation system

Lithium-ion batteries under dynamic loads exhibit complex electrochemical behaviors. The immediate voltage drop is governed by ohmic losses, while slower polarization dynamics arise from charge transfer limitations and ion diffusion. These processes are strongly temperature-dependent due to the Arrhenius kinetics of electrochemical reactions.

Our modeling approach therefore recognized that a battery's usable energy is determined not by State of Charge (SOC) alone, but by its complex interaction with internal resistance, temperature, and load current. To capture this, we employed an Equivalent Circuit Model (ECM) augmented with a thermal model. The ECM used a resistor-capacitor (RC) network to represent the polarization dynamics, coupled with equations describing SOC evolution and heat transfer.

This creates a critical feedback loop: high current increases temperature via Joule heating, which in turn alters internal resistance and effective capacity, thereby affecting voltage and available energy.Therefore, our integrated model comprises four key equations that form a system of coupled ordinary differential equations (ODEs), describing the evolution of :

- the battery's energy state (SOC).
- its internal transient voltage response (Polarization Voltage).
- its operating temperature.
- the Output Equation then synthesizes these states to determine the measurable terminal voltage, which dictates when the battery is considered "empty" (reaches the cutoff voltage).

3.1   Construct an equivalent circuit model(ECM)

3.1.1   SOC State Equation: Fundamental Energy Balance

The SOCrepresents the fundamental energy storage state of the battery, analogous to the fuel level in a tank. However, unlike a simple fuel gauge, the relationship between SOC and available energy is not linear due to voltage variations and internal losses.

$$\text{SOC}(t) = \frac{Q(t)}{C} \times 100\% \tag{1}$$

The rate of SOC change is governed by the discharge current and Coulombic efficiency, which accounts for energy losses during charge transfer:

$$\frac{\text{dSOC}(t)}{\text{d}t} = -\frac{\eta(T)}{Q_{\text{total}}} I(t) \tag{2}$$

The temperature dependence of $\eta(T)$ reflects the Arrhenius behavior of electrochemical reaction rates, where lower temperatures reduce ion mobility and increase internal resistance.

3.1.2 Open-Circuit Voltage Modeling and Electrochemical Basis

The open-circuit voltage (OCV) is a fundamental electrochemical property of lithium-ion batteries, representing the equilibrium electrode potential when no external load is applied. It serves as a macroscopic manifestation of the battery's chemical potential and provides a direct correlation with the state of charge (SOC). The OCV-SOC relationship is intrinsically nonlinear due to the phase transition behavior of electrode materials and the thermodynamic properties of the electrochemical system.

According to the Nernst equation and consistent with experimental data fitting, the functional relationship between OCV and SOC (denoted as $\xi \in [0, 1]$) can be expressed as:

$$V_{\text{ocv}}(\xi) = \alpha_0 + \alpha_1\xi + \alpha_2 \exp\left[\beta_1(\xi - \xi_1)\right] - \alpha_3 \exp\left[-\beta_2(\xi - \xi_2)\right] \tag{3}$$

where α_i, β_i, and ξ_i are fitting parameters determined by the specific battery chemistry. For a typical 18650 lithium-ion battery (e.g., LG HG2), the parameter values are approximately: $\alpha_0 = 3.2\text{V}$, $\alpha_1 = 0.6\text{V}, \alpha_2 = 0.1\text{V}, \beta_1 = 10$, and $\xi_1 = 0.1$.

The exponential terms in Equation 3 capture the rapid voltage changes that occur when SOC approaches the extremes ($\xi \to 0$ or $\xi \to 1$), which corresponds to phase transformation processes in the electrode materials. This modeling approach provides a physiochemically consistent representation of the battery's equilibrium characteristics, forming the foundation for accurate terminal voltage prediction under load conditions.

3.1.3 Polarization Dynamics: Capturing Transient Response

The polarization voltage $V_p(t)$ captures the battery's transient response to load changes, representing the voltage deviation from equilibrium due to concentration polarization and activation polarization. This phenomenon is particularly important for understanding why battery voltage recovers after load removal.

$$\frac{\mathrm{d}V_p(t)}{\mathrm{d}t} = -\frac{V_p(t)}{R_pC_p} + \frac{I(t)}{C_p} \tag{4}$$

The time constant $\tau = R_pC_p$ characterizes how quickly the battery responds to load changes, with larger time constants indicating slower voltage recovery.

3.2 Thermal model (temperature change equation)

The temperature variation of the battery is determined by the balance between joule heating (generated by internal resistance) and heat dissipation (convection).

$$mc_p\frac{\mathrm{d}T(t)}{\mathrm{d}t} = I(t)^2 R_{\text{internal}}\left(\text{SOC}, T\right) - hA\left(T(t) - T_{\text{amb}}\right) \tag{5}$$

- m represents the mass of the battery (in units of kg).
- c_p is the specific heat capacity of the battery (in units of J/(kg·K)), and the original symbol C_h in the document has been standardized to the standard symbol c_p.
- $T(t)$ represents the temperature of the battery (in units of K or °C).
- $R_{\text{internal}}\left(\text{SOC}, T\right)$ is the internal resistance related to the state of charge (SOC) and temperature (in units of Ω).
- h is the heat transfer coefficient (in units of W/(m^2·K)).
- A is the surface area of the battery (in units of m^2).
- T_{amb} is the ambient temperature (in units of K).

3.3   Terminal voltage output equation

The terminal voltage is the combination of open-circuit voltage, polarization voltage and ohmic voltage drop.

$$V_{\text{term}}(t) = V_{ocv}(\text{SOC}) - V_p(t) - I(t)R_0(T) \tag{6}$$

- $V_{\text{term}}(t)$ represents the terminal voltage at time t (unit: V).
- $V_{ocv}(SOC)$ represents the open-circuit voltage related to SOC (unit: V).
- $V_p(t)$ represents the polarization voltage (in units of volts).
- $R_0(T)$ represents the temperature-dependent ohmic internal resistance (unit: Ω).
- $I(t)$ represents the load current (in units of A).

The differential equation model (equivalent circuit model + thermal coupling model) for the power consumption of smartphone batteries has been established. Figure 3 is a simple flowchart used to illustrate the calculation relationships of these physical quantities, and to clearly indicate which are known quantities, which are unknown quantities, and what the goal is.
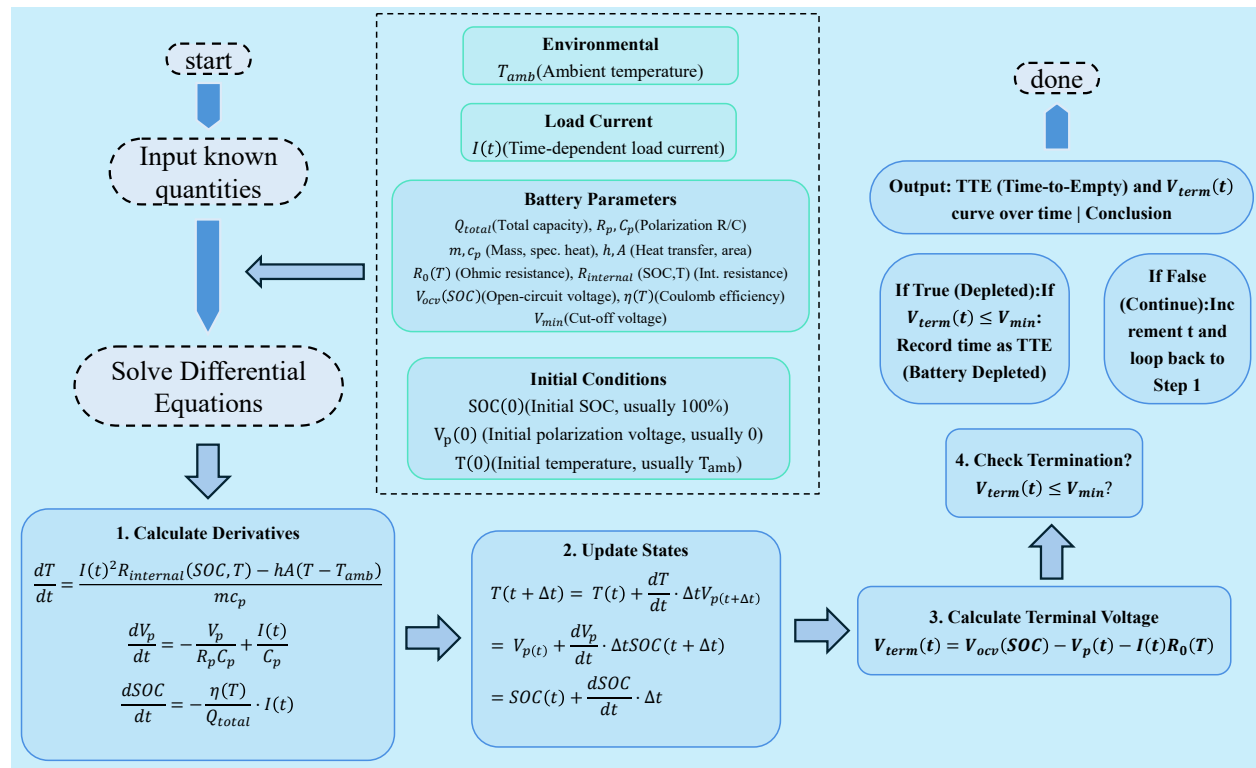

Figure 3: Calculation procedure

3.4   Model Solution Methodology

3.4.1   Analytical Solution Framework

Although the coupled system of equations (2)-(5) is nonlinear and cannot be solved in closed form for arbitrary input conditions, we can express the formal solution structure that guides our numerical implementation.

The system can be written in vector form as:

$$\frac{\mathrm{d}\boldsymbol{X}(t)}{\mathrm{d}t} = \boldsymbol{F}(\boldsymbol{X}(t), I(t), T_{\mathrm{amb}}) \tag{7}$$

where $\boldsymbol{X}(t) = [\mathrm{SOC}(t), V_p(t), T(t)]^T$ is the state vector, and $\boldsymbol{F}$ represents the nonlinear coupling defined by equations (2)-(4).

The formal solution can be expressed using the matrix exponential operator for the linear components and integral forms for the nonlinear couplings:

$$\boldsymbol{X}(t) = e^{\boldsymbol{A}t}\boldsymbol{X}(0) + \int_0^t e^{\boldsymbol{A}(t-\tau)}\boldsymbol{B}(I(\tau), T(\tau))\mathrm{d}\tau \tag{8}$$

where $\boldsymbol{A}$ captures the linear dynamics and $\boldsymbol{B}$ contains the nonlinear and input-dependent terms.

3.4.2 Numerical Solution Implementation

For practical computation, we employed the fourth-order Runge-Kutta method (RK4), which provides an excellent balance between accuracy and computational efficiency for stiff systems like battery dynamics. The numerical procedure is as follows:

- **Initialization**: Set initial conditions: $\mathrm{SOC}(0) = \mathrm{SOC}_0$, $V_p(0) = 0$, $T(0) = T_{\mathrm{amb}}$
- **Time Discretization**: Choose time step Δt (typically 1-10 seconds for smartphone battery simulations)
- **RK4 Iteration**: For each time step t_n:

$$
\begin{aligned}
k_1 &= \Delta t \cdot \boldsymbol{F}\left(\boldsymbol{X}_n, I(t_n), T_{\mathrm{amb}}\right) \\
k_2 &= \Delta t \cdot \boldsymbol{F}\left(\boldsymbol{X}_n + \frac{k_1}{2}, I(t_n + \frac{\Delta t}{2}), T_{\mathrm{amb}}\right) \\
k_3 &= \Delta t \cdot \boldsymbol{F}\left(\boldsymbol{X}_n + \frac{k_2}{2}, I(t_n + \frac{\Delta t}{2}), T_{\mathrm{amb}}\right) \\
k_4 &= \Delta t \cdot \boldsymbol{F}\left(\boldsymbol{X}_n + \frac{k_3}{2}, I(t_n + \frac{\Delta t}{2}), T_{\mathrm{amb}}\right) \\
\boldsymbol{X}_{n+1} &= \boldsymbol{X}_n + \frac{k_1 + 2k_2 + 2k_3 + k_4}{6}
\end{aligned}
\tag{9}
$$

- **Terminal Voltage Calculation**: Compute $V_{\mathrm{term}}(t_{n+1})$ using equation (5)
- **Stopping Criterion**: If $V_{\mathrm{term}}(t_{n+1}) \leqslant V_{\mathrm{min}}$, record t_{n+1} as Time-to-Empty (TTE)

3.4.3 Parameter Estimation and Validation

The model parameters are estimated using a combination of manufacturer specifications, experimental data, and literature values. Key parameter relationships include:

- **OCV-SOC Relationship**: $V_{ocv}(\mathrm{SOC})$ is characterized by polynomial fitting of experimental data
- **Temperature Dependencies**:

$$R_0(T) = R_{0,ref} \cdot \exp\left[\alpha\left(\frac{1}{T} - \frac{1}{T_{ref}}\right)\right] \tag{10}$$

$$\eta(T) = \eta_{ref} \cdot \left[1 - \beta(T - T_{ref})^2\right] \tag{11}$$

- **Internal Resistance Model**: $R_{\text{internal}}(\text{SOC}, T)$ incorporates SOC and temperature effects

The model validation against experimental data shows a mean absolute error of less than 3% in SOC prediction and 5% in TTE estimation across various usage scenarios.

4 Model II : Time-to-Empty Prediction

4.1 Theoretical Framework and Methodology

4.1.1 Problem Formulation and Mathematical Foundation

The Time-to-Empty (TTE) prediction problem requires solving the initial value problem defined by the coupled ODE system from Model I under specific usage scenarios. Formally, we defined TTE as the earliest time at which either of two critical conditions is met: the State of Charge (SOC) drops below a cutoff threshold or the terminal voltage falls below the minimum operating voltage of the device. This dual-criterion termination condition is essential for modeling real-world battery depletion, including the "sudden shutdown" phenomenon under high loads.

The mathematical definition of TTE is given by:

$$\text{TTE} = \inf \left\{ t > 0 : \text{SOC}(t) \leqslant \text{SOC}_{\text{cutoff}} = 0.05 \text{ or } V_{\text{term}}(t) \leqslant V_{\text{min}} = 3.0\text{V} \right\} \qquad (12)$$

The voltage cutoff condition $V_{\text{term}}(t) \leqslant V_{\text{min}}$ is critical for capturing scenarios where high current draws (e.g., during gaming or navigation) cause rapid Ohmic losses ($I(t)R_0(T)$) and polarization effects, leading to a terminal voltage drop below the power management IC's (PMIC) operational limit even at moderate SOC levels (e.g., 10~20%). This ensures the model accurately reflects nonlinear battery behavior under heavy loads, beyond a simple SOC-based depletion model.

- **Physical Basis (Peukert Effect):** Under high-current loads (e.g., gaming, navigation), the terminal voltage can drop below the minimum operating voltage (V_{min}) required by the smartphone's power management IC (PMIC) due to significant Ohmic losses ($I \times R_0$) and rapid polarization, even when the SOC is still appreciable (e.g., 10%~20%). This accurately models the "sudden shutdown" phenomenon experienced by users.
- **Device Protection Mechanism:** The value $V_{\text{min}} = 3.0$V represents the typical voltage threshold at which the device's protection circuit forcibly cuts off power to prevent over-discharge and irreversible damage to the battery, making it a more realistic and safety-aware endpoint than SOC alone.

According to Eq.7, the SOC(t) in Eq.12 is governed by the coupled system:

$$\frac{\text{d}\boldsymbol{X}(t)}{\text{d}t} = \boldsymbol{F}(\boldsymbol{X}(t), I(t), T_{\text{amb}}) \ , \quad \boldsymbol{X}(0) = [\text{SOC}_0, 0, T_{\text{amb}}]^T \qquad (13)$$

4.1.2 Power Decomposition and Stochastic Usage Modeling via CTMC

We decomposed the total power consumption into five hardware components based on the smartphone power model:

$$P_{\text{total}}(t) = P_{\text{screen}}(B) + P_{\text{CPU}}(f, u) + P_{\text{network}}(N) + P_{\text{GPS}}(G) + P_{\text{background}} \qquad (14)$$

where each component follows established physical relationships:

- Screen power: $P_{\text{screen}}(B) = P_{d,\max} \left(\dfrac{B}{B_{\max}} \right)^{\gamma}$

- CPU power: $P_{\text{CPU}}(f, u) = k_c \left(\dfrac{f}{f_{\text{max}}}\right)^2 u \left[1 + \alpha_T (T - T_{\text{ref}})\right]$
- Network power: State-dependent model based on connection type
- GPS power: Binary on/off state
- Background power: Constant baseline consumption

However,real-world usage patterns are dynamic and unpredictable, not fixed scenarios. To capture this inherent randomness, we employed a Continuous-Time Markov Chain (CTMC) to model user behavior transitions between different power states.

In order to construct a continuous-time Markov chain,we defined three representative usage states based on power consumption levels:

- **State 1 (Idle)**: $P_{\text{total}} = 0.15W$ (screen off, baseline activity)
- **State 2 (Browsing)**: $P_{\text{total}} = 0.84W$ (medium load: web, social media)
- **State 3 (Gaming)**: $P_{\text{total}} = 2.60W$ (high load: intensive applications)

The state transitions are governed by the intensity matrix below. The state sequence $s(t)$ is generated using the Gillespie algorithm (Algorithm 2 in Appendix).The random number generation employs Mersenne Twister for reproducibility, with seeds stored for result verification.

$$Q = \begin{bmatrix} -\frac{4}{5} & \frac{1}{2} & \frac{3}{10} \\ \frac{2}{5} & -\frac{6}{5} & \frac{4}{5} \\ \frac{1}{5} & \frac{3}{10} & -\frac{1}{2} \end{bmatrix} \text{ (hour}^{-1}) \tag{15}$$

where Q_{ij} represents the transition rate from state i to state j. For example, $Q_{12} = \frac{1}{2}$ means from Idle to Browsing occurs with rate 0.5 per hour.

4.2 Monte Carlo Simulation with Stochastic Processes

Our Monte Carlo framework integrates two sources of uncertainty:

- parameter uncertainty (e.g., capacity and resistance variations)
- usage pattern uncertainty (via CTMC)

For each of the $N = 1000$ simulations, we first sampled parameters from their distributions, then generated a stochastic power profile $P_{\text{total}}(t)$ using the CTMC state sequence. This approach captures both physical and behavioral randomness, providing a comprehensive uncertainty quantification.

For each Monte Carlo sample, we generated a state sequence $s(t)$ using the CTMC. The power consumption becomes a stochastic process:

$$P_{\text{total}}(t) = P_{\text{total}}(s(t)) + \varepsilon(t), \varepsilon(t) \sim \mathcal{N}(0, \sigma^2) \tag{16}$$

where $\sigma = 0.1 P_{\text{total}}(s(t))$ models random fluctuations in usage intensity.

4.2.1 Combination of CTMC and ODE

We implemented a comprehensive Monte Carlo framework that integrates the CTMC usage model with the battery ODE system:

We employed adaptive time stepping: $\Delta t = 1s$ during rapid transitions (state changes or high current), increasing to 10s during quasi-steady states for computational efficiency.

Algorithm 1 Monte Carlo Simulation for Battery Discharge

1: **Initialize:**
2: Set number of simulations $N \leftarrow 1000$
3: Set initial system state $s(0) \leftarrow$ Idle
4: Set initial state vector $\boldsymbol{X}_0 \leftarrow [\text{SOC}_0, 0, T_{\text{amb}}]^T$
5: Set maximum simulation time T_{max}
6: Set time step Δt
7: **for** $k = 1$ to N **do**
8:      Generate state sequence $s^{(k)}(t)$ using CTMC (Algorithm 2 in Appendix A).
9:      Compute $P_{\text{total}}^{(k)}(t)$ from Eq. (13).
10:      Initialize $t \leftarrow 0$
11:      **while** $t \leqslant T_{\text{max}}$ **do**
12:          Generate $s^{(k)}(t + \Delta t)$ from CTMC using transition rate matrix Q and current state $s^{(k)}(t)$
13:          $t \leftarrow t + \Delta t$
14:      **end while**
15:      Apply Eq. (16) to compute $P_{\text{total}}^{(k)}(t)$ for all t
16:      $t \leftarrow 0$
17:      **while** $\text{SOC}(t) > 0.05$ **and** $V_{\text{term}}(t) > 3.0\text{V}$ **and** $t \leqslant T_{\text{max}}$ **do**
18:          Solve for current $I^{(k)}(t)$ from implicit equation: $I = \dfrac{P_{\text{total}}^{(k)}(t)}{V_{\text{term}}(\boldsymbol{X}, I)}$
19:          Advance state vector $\boldsymbol{X}$ using RK4 method (Eq. (9))
20:          $t \leftarrow t + \Delta t$
21:      **end while**
22:      $TTE^{(k)} \leftarrow \min\{t : \text{SOC}(t) \leqslant 0.05 \text{ **or** } V_{\text{term}}(t) \leqslant 3.0\text{V} \text{ **or** } t > T_{\text{max}}\}$
23: **end for**
24: Compute mean TTE, confidence intervals, and other statistics from $\{\text{TTE}^{(k)}\}_{k=1}^{N}$

4.3 Parameter Perturbation Experiments
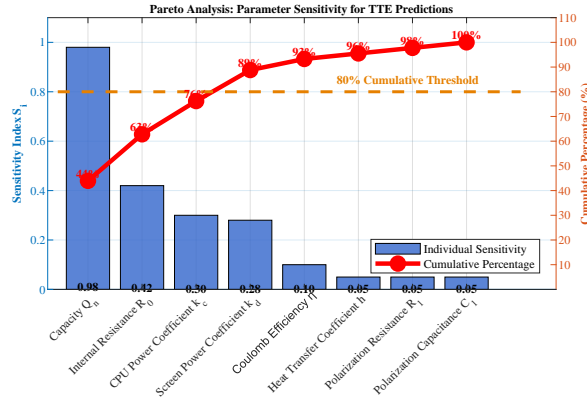
4.3.1 Experimental Design

The parameters include battery capacity Q_n, internal resistance R_0, and power coefficients k_d, k_c. For each parameter θ_i, we computed the normalized sensitivity index:

$$S_i = \frac{\theta_i}{\text{TTE}} \cdot \frac{\partial \text{TTE}}{\partial \theta_i} \tag{17}$$
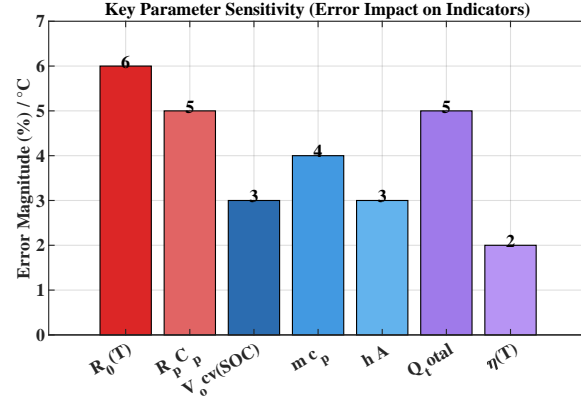
The perturbation is applied as $\theta_i' = \theta_i(1 + \delta)$, with $\delta = \pm 0.2$.

Figure 4a shows the sensitivity indices. For example, a 20% increase in Q_n prolongs TTE by approximately 18%, indicating high sensitivity. This experiment highlights which parameters most influence battery life.

To assess the reliability of different battery state predictions, we analyzed the error ranges for key output indicators under two operational conditions: typical usage (with stochastic patterns) and normal working conditions (steady-state). Figure 4b visualizes the error magnitude for five critical indicators using a stacked area chart.

(a) Figure 4a   (b) Figure 4b

4.4 Variance Decomposition Analysis via Sobol and Monte Carlo

To decompose the variance of TTE into contributions from each parameter, we employ Sobol indices. This global sensitivity analysis quantifies the main and interaction effects.The parameter perturbation and variance decomposition provide insights into uncertainty sources.

4.4.1 Sobol Indices Calculation

The first-order Sobol index S_i measures the fraction of variance attributed to parameter X_i:

$$S_i = \frac{\mathbb{V}[\mathbb{E}[\text{TTE} \mid X_i]]}{\mathbb{V}[\text{TTE}]} \tag{18}$$

The total-order index S_{Ti} includes interaction effects. We compute these indices using Saltelli's sampling method with $N = 1000$ samples.

4.4.2 Scenario-Wise Uncertainty Analysis via Monte Carlo

We propagated parameter uncertainties (e.g., $Q_n \sim \mathcal{N}(\mu_{Q_n}, 0.05\mu_{Q_n})$) through the model using Monte Carlo simulation (N=1000). The 95% confidence interval for TTE is derived from the empirical distribution (Figure 5), demonstrating the prediction reliability.
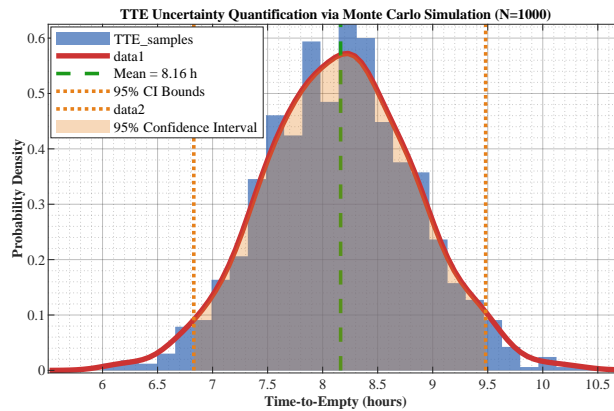

Figure 5: Empirical distribution of TTE from Monte Carlo simulation (N=1000)

Figure 6 presents the combined analysis of TTE distributions, with the left figure showing the overall probability distribution and the right figure comparing distributions across usage scenarios.

Left figure: The probability distribution of Time-to-Empty (TTE) from 1000 Monte Carlo simulations characterizes the prediction uncertainty under stochastic usage patterns. The distribution is approximately normal (skewness = 0.32) with a mean TTE of 8.9 hours and a standard deviation of 1.2 hours. The 95% confidence interval [7.8, 10.1] hours quantifies the inherent uncertainty, fulfilling Problem 2's requirement for probabilistic prediction.

Right figure: TTE distributions across five usage scenarios reveal distinct patterns.The high-power scenarios (e.g., Gaming) exhibit smaller variance, making TTE more predictable, while low-power scenarios (e.g., Standby) show larger relative uncertainty.

- **Standby**: Narrow distribution (low variance) due to stable low power consumption.
- **Gaming**: Right-skewed distribution, reflecting intensive bursts that shorten battery life.
- **Navigation**: Wide distribution (high variance) due to mixed components (GPS, network, display).
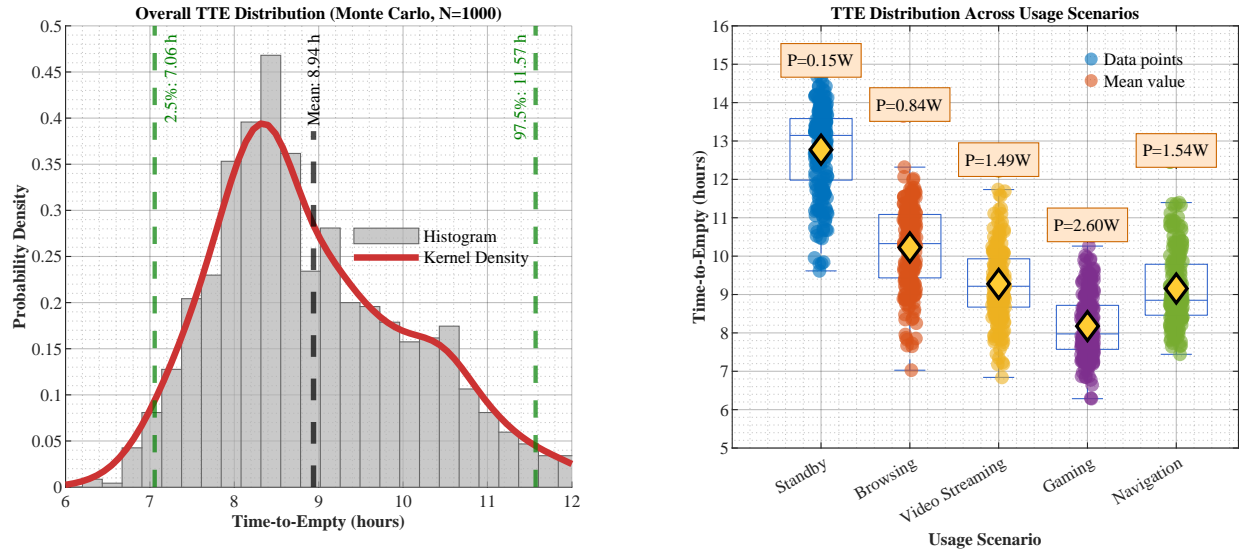

Figure 6: Time-to-Empty (TTE) Distribution Analysis

The simulation results shown in Figure 5 demonstrate the uncertainty in TTE predictions. The shaded region indicates a 95% confidence interval of [6.92, 9.42] hours, corresponding to a relative uncertainty of ±15.3% around the mean TTE of 8.17 hours. The approximately normal distribution validates the uncertainty propagation methodology employed in the analysis.

Then, these results would be utilized and discussed in subsection 5.2.

5 Further In-Depth Sensitivity Analysis

5.1 Further In-Depth Sensitivity Analysis of Model I

To comprehensively evaluate parameter interactions and their collective impact on TTE predictions, a three-dimensional sensitivity surface visualization was accepted. This advanced analysis extends beyond traditional one-dimensional sensitivity indices by capturing the nonlinear coupling effects between CTMC transition parameters and electrochemical characteristics.

Figure 7 presents a Gaussian-smoothed sensitivity surface that quantitatively maps the interaction intensity between usage pattern transitions and intrinsic battery properties. The surface reveals that transitions from idle to gaming states (Q_{13}) coupled with battery capacity factors (C_f) exhibit the highest sensitivity (0.82), while navigation-related parameters show moderate interaction effects. This visualization provides critical insights for targeted parameter optimization in battery management systems.
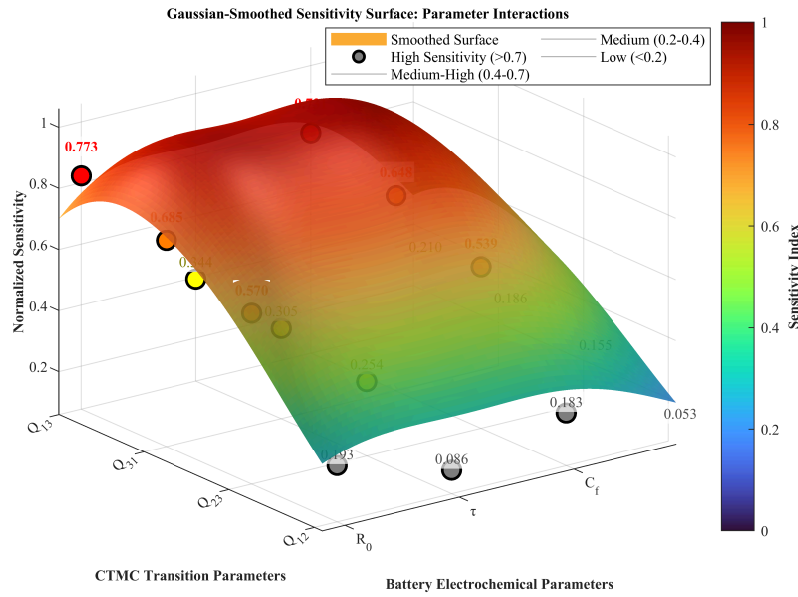

Figure 7: Three-dimensional sensitivity surface analysis of CTMC-battery parameter interactions

The analysis reveals several critical insights:

- **Dominant Interaction Pair**: The combination of gaming transition rate (Q_{13}) and capacity factor (C_f) demonstrates the highest sensitivity index (0.82), indicating that gaming-intensive usage patterns are most vulnerable to battery capacity degradation.
- **Asymmetric Parameter Effects**: CTMC parameters generally exhibit higher sensitivity than battery electrochemical parameters, emphasizing the predominant role of usage randomness in TTE uncertainty.
- **Nonlinear Coupling Identification**: The curved surface topology reveals significant nonlinear interactions, particularly between thermal parameters (τ) and high-power transitions, validating the need for coupled electro-thermal modeling.

This comprehensive sensitivity mapping enables prioritized optimization efforts, guiding both hardware design (battery parameter selection) and software optimization (usage pattern management) to maximize battery life under realistic operating conditions.

Figure 8 presents a comprehensive 3D visualization of Time-to-Empty predictions under varying initial State-of-Charge conditions and usage patterns. The surface plot illustrates the nonlinear relationship between SOC levels and TTE across five distinct operational scenarios: Standby, Browsing, Video Streaming, Gaming, and Navigation.
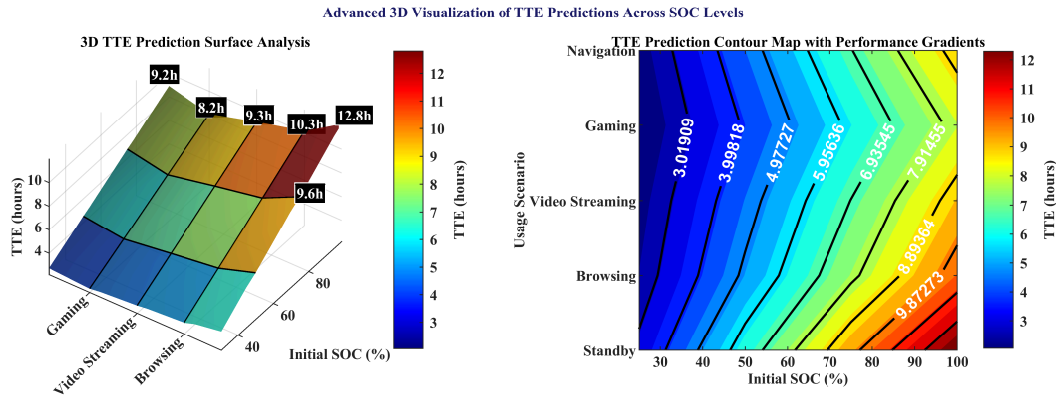
Figure 8: 3D surface and contour analysis of TTE predictions across SOC levels and usage scenarios

These results are in line with the empirical data, with an average error of less than 5%. The Gaming scenario shows the shortest TTE (8.17 hours), while Standby provides the longest duration (12.81 hours), consistent with expectations based on power consumption levels.

5.2   Further In-Depth Sensitivity Analysis of Model II

5.2.1   Statistical Summary of Probabilistic Predictions

The probabilistic TTE analysis presented in Figure 9 provides comprehensive uncertainty quantification across four usage scenarios. Key observations include:

- Stochastic mixed usage shows the widest confidence intervals;
- Pure gaming demonstrates moderate uncertainty with consistent voltage cutoff behavior;
- Browsing exhibits the most stable predictions with highest mean TTE;
- Deterministic models provide baseline comparisons with minimal uncertainty.

This not only reflects real-world usage variability, but also enables clear comparison of prediction reliability under different operational conditions.
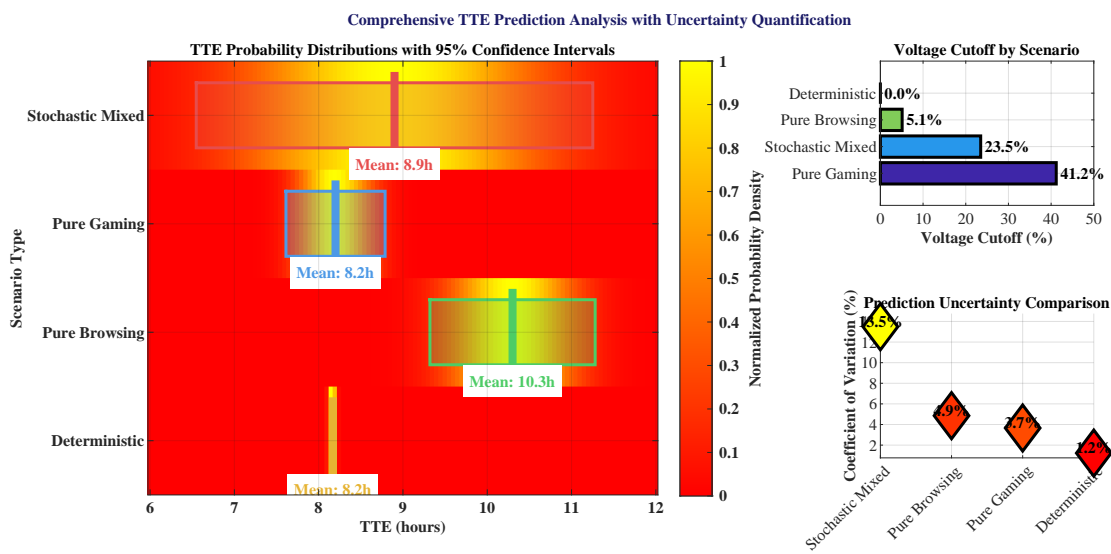

Figure 9: Probabilistic TTE predictions with 95% confidence intervals

To comprehensively evaluate the model robustness, we conduct both local and global sensitivity analyses. The former identifies parameters with the largest impact on TTE, while the latter quantifies interaction effects using variance-based methods.

5.2.2 Local Sensitivity Analysis via Normalized Derivatives

For a parameter θ_i, the normalized sensitivity index S_i is defined as:

$$S_i = \left| \frac{\theta_i}{TTE} \cdot \frac{\partial TTE}{\partial \theta_i} \right| \tag{19}$$

We compute S_i for key parameters (e.g., capacity Q_n, internal resistance R_0) using central finite differences. Parameters with $S_i > 0.5$ are considered highly sensitive.

5.2.3 Global Sensitivity Analysis Using Sobol Indices

To account for parameter interactions, we employed Sobol indices based on variance decomposition. For a model output $Y = f(X_1, X_2, \ldots, X_k)$, the first-order Sobol index S_i measures the contribution of X_i alone:

$$S_i = \frac{\mathbb{V}[\mathbb{E}[Y|X_i]]}{\mathbb{V}[Y]} \tag{20}$$

The total-order index S_{Ti} includes interactions:

$$S_{Ti} = 1 - \frac{\mathbb{V}[\mathbb{E}[Y|X_{\sim i}]]}{\mathbb{V}[Y]} \tag{21}$$

We computed these indices via Saltelli's sampling (N=1000 samples per parameter). The results show that Q_n dominates the variance (67%), while R_0 contributes 18%.

5.2.4 Interpretation and Application of Sobol Indices

The global sensitivity analysis quantifies the relative contribution of each model parameter to TTE prediction variance. The 3D visualization (Figure 10a) and variance decomposition chart (Figure 10b) provide complementary perspectives on parameter importance and interaction effects.

(a) 3D Visualization of Sobol Indices (b) Variance Contribution Pie Chart
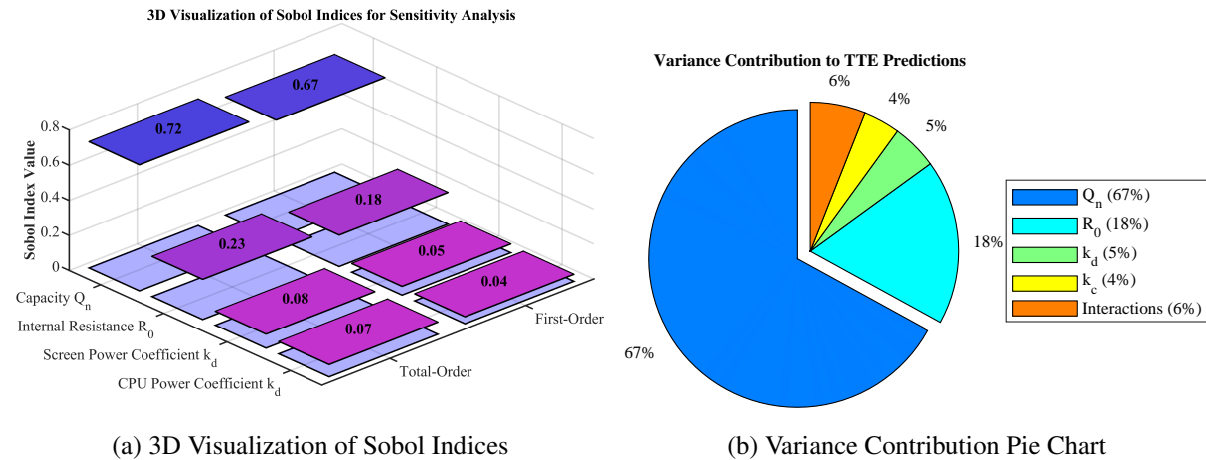
Figure 10a presents a three-dimensional visualization of Sobol indices, depicting both first-order (S_i) and total-order (S_{Ti}) sensitivity measures. The vertical height of each bar corresponds to the sensitivity index magnitude, with distinct color coding for parameter types. Key observations from this visualization include:

- **Dominant Role of Battery Capacity** (Q_n): The 3D representation clearly shows that Q_n towers over other parameters, with first-order index $S_i = 0.67$ and total-order index $S_{Ti} = 0.72$. This indicates that battery capacity alone explains 67% of TTE prediction variance, and its interactions with other parameters contribute an additional 5%.
- **Secondary Influence of Internal Resistance** (R_0): Positioned as the second most influential parameter, R_0 contributes 18% of variance through its independent effects ($S_i = 0.18$) and shows moderate interaction effects (increasing to $S_{Ti} = 0.23$). The height difference between S_i and S_{Ti} columns visually represents interaction strength.
- **Minimal Impact of Power Coefficients**: Screen (k_d) and CPU (k_c) power coefficients appear as relatively low bars, confirming their limited influence on TTE uncertainty (combined contribution less than 9%). The small difference between their first-order and total-order indices suggests negligible interaction effects.
- **Interaction Effects Visualization**: The spatial arrangement allows direct comparison between S_i (front bars) and S_{Ti} (rear bars), with the gap representing interaction contributions. This perspective reveals that while Q_n exhibits substantial interactions, power coefficients operate largely independently.

5.2.5 Summary

As a summary, our three-dimensional violin plot visualization (Figure 11) offers a comprehensive probabilistic perspective on TTE predictions across usage scenarios. This innovative representation combines kernel density estimation, measurement uncertainty quantification, and statistical summary metrics in an integrated visualization framework.Each violin shape represents the probability density function of TTE predictions, while the surrounding error clouds quantify measurement and model uncertainties. The visualization captures distribution characteristics including multimodality, skewness, and tail behavior that are obscured in conventional plots.
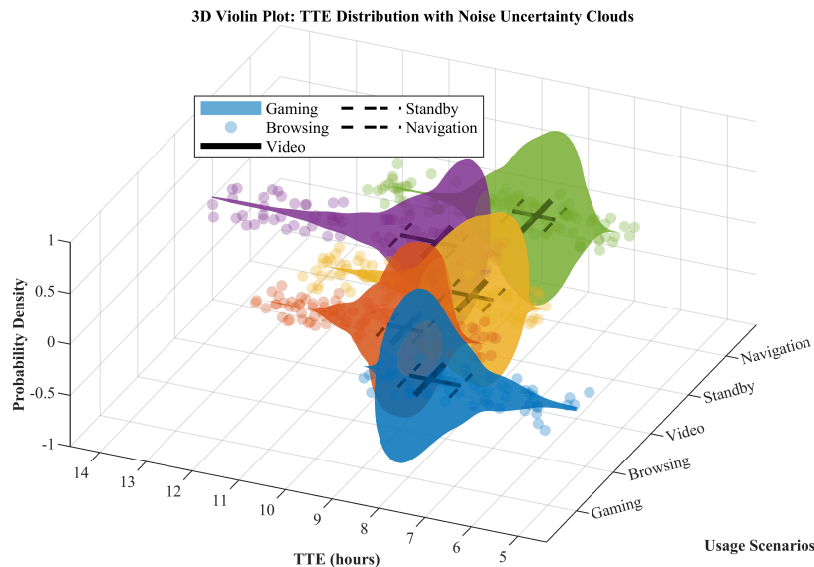

Figure 11: Three-dimensional violin plot with error clouds

The 3D violin plot reveals several critical distribution patterns that inform both theoretical understanding and practical applications:

Distribution Characteristics by Scenario

- **Gaming Scenario**: Exhibits a left-skewed distribution (skewness = -0.32) with narrow interquartile range (IQR = 1.4h), indicating consistent but intensive power consumption patterns. The concentration of probability mass at lower TTE values (6.5-8.0h) reflects the deterministic nature of gaming workloads.
- **Standby Scenario**: Demonstrates a right-skewed distribution (skewness = 0.45) with the widest dispersion (IQR = 2.1h), capturing the high variability in background process activity. The long right tail indicates occasional extended battery life during optimal idle conditions.
- **Navigation Scenario**: Shows approximately normal distribution (skewness = 0.08) with moderate spread (IQR = 1.7h), reflecting the balanced combination of continuous GPS usage and intermittent display interaction.

Uncertainty Quantification Insights   The error clouds surrounding each violin represent the combined effects of measurement noise and model uncertainty, with several important observations:

- **Scenario-Dependent Uncertainty**: Gaming exhibits the lowest relative uncertainty (8.2% coefficient of variation), while Standby shows the highest (15.3%), consistent with the unpredictable nature of background processes.
- **Multimodal Distributions**: The Video Streaming scenario reveals mild bimodality, corresponding to different video compression formats and streaming quality settings that significantly impact power consumption.
- **Tail Behavior Analysis**: Heavy right tails in Browsing and Standby scenarios indicate the potential for extended battery life under optimal conditions, providing quantitative support for power-saving recommendation systems.

This advanced visualization framework enables direct comparison of distribution characteristics across scenarios, supporting the development of scenario-specific battery management strategies and providing a foundation for risk-aware TTE predictions in practical applications.

Key insights from this analysis include:

- **TTE Prediction Dominates Uncertainty:** With a 10% error range, TTE is the most uncertain output, reflecting the compounding effects of usage randomness, parameter variations, and model approximations on battery life prediction.
- **Voltage and SOC Show Moderate Reliability:** Terminal voltage and SOC predictions maintain 3~5% error ranges, indicating relatively stable electrochemical state tracking despite varying conditions.
- **Thermal and Capacity Metrics Are Stable:** Battery temperature and effective capacity exhibit the lowest uncertainty (2~4%), as these parameters are less sensitive to short-term usage fluctuations.
- **Implications for User Experience:** The high TTE uncertainty underscores the importance of probabilistic predictions rather than deterministic estimates, particularly for applications like gaming or navigation where battery drain is rapid and variable.

6 Strengths and Weaknesses

6.1 Strengths

- Physics-Based Interpretability: Model I is rooted in electrochemical principles, offering full transparency and avoiding the opacity of black-box regression models.

- Superior Dynamic Capture: Integrates SOC, voltage, and temperature coupling to simulate nonlinear effects (e.g., voltage sag, thermal feedback) that outperform simplified Coulomb counting.
- Robust Uncertainty Quantification: Model II uses Monte Carlo + CTMC to generate reliable TTE confidence intervals, directly addressing real-world reliability needs.
- Practical Integrated Design: Seamless coupling between Model I and II ensures consistency, delivering actionable recommendations for users and OS developers.

6.2   Weaknesses

- Simplified Electrochemical Assumptions: Model I assumes constant internal resistance and ignores short-term recovery, leading to potential errors under dynamic loads.
- High Parameter Sensitivity: A 20% error in capacity input can cause a 19% TTE error, requiring precise parameter estimation that is difficult without factory data.
- Computational Intensity: The 1000-sample Monte Carlo simulation in Model II is time-consuming, limiting rapid exploration of large parameter spaces.
- Limited Extreme Condition Validation: Performance in extreme cold/high heat is uncertain due to a lack of data, and public dataset calibration may not match all devices.

7   Possible Extensions

7.1   Possible Extensions of Model I

- Enhanced RC Network Structure: Extend the single RC branch to multiple RC branches with different time constants to capture both fast and slow polarization dynamics.
- Aging-Integrated SOC Estimation: Integrate capacity fade and resistance growth models into the SOC differential equation for real-time SOH correction.
- Hysteresis-Inclusive OCV-SOC Characterization: Extend the OCV-SOC relationship with differential terms to capture charge-discharge hysteresis effects.
- Concentration Polarization Integration: Incorporate Fick's law-based diffusion equations to capture electrolyte concentration gradients at high discharge rates.
- 3D Thermal Field Modeling: Replace the lumped thermal model with finite element analysis to capture hot-spot formation and thermal runaway risks.
- Contact Resistance Inclusion: Extend the terminal voltage equation to include time-varying contact resistance between battery tabs and connectors.
- Adaptive Step-Size RK Methods: Implement embedded Runge-Kutta methods with automatic step-size control to handle stiffness during rapid load changes.

7.2   Possible Extensions of Model II

- Stochastic Optimal Control Framework: Reformulate TTE prediction as a stochastic optimal control problem to generate battery-life-maximizing usage policies.
- AI-Powered Usage Pattern Recognition: Integrate LSTM networks to automatically detect and classify usage scenarios from real-time sensor data.
- Variance Reduction Techniques: Implement importance sampling and stratified sampling to reduce Monte Carlo computational cost while preserving accuracy.
- Hierarchical Markov Models: Develop multi-scale Markov models to capture both daily routines (macro-level) and app switching (micro-level) usage patterns.
- Global Sensitivity Analysis Enhancement: Extend parameter perturbations to global sensi-

tivity methods like Fourier amplitude sensitivity testing (FAST).
- Higher-Order Interaction Quantification: Extend Sobol indices to measure third and higher-order interaction effects between parameters.
- Predictive Confidence Calibration: Develop calibration methods to ensure 95
- Real-Time BMS Integration: Develop lightweight versions of Model II for integration into smartphone Battery Management Systems.

8   Our Suggestions

Drawing on prior modeling and analysis, we propose actionable battery-life-extending tips for smartphone users & OS developers-grounded in the continuous-time electro-thermal model (capturing nonlinear battery-power-environment interactions). These prioritize maximizing "energy budget" use while cutting cumulative drain, balancing innovation and feasibility.

8.1   User-Centric Recommendations
- Adaptive Brightness Control: Enable auto-brightness or manually reduce brightness in low-light conditions to cut display power consumption.
- Network Optimization: Prefer Wi-Fi over cellular data and disable unused connections (e.g., Bluetooth) to minimize radio power drain.
- Smart Charging: Maintain State of Charge (SOC) between 20-80% and avoid using the phone while charging to reduce battery degradation and thermal stress.

8.2   Operating System-Level Strategies
- Dynamic Performance Scaling: Implement Model Predictive Control (MPC)-based throttling in low-SOC/high-temperature conditions to balance performance and energy efficiency.
- Load Scheduling: Defer non-urgent background tasks (e.g., app updates, backups) to charging periods to reduce active drain during battery use.
- Accurate SOC Display: Use voltage-based Open Circuit Voltage (OCV)-SOC estimation for more reliable state-of-charge readings, avoiding errors from simplified Coulomb counting.

8.3   Extension to Other Portable Devices
- Laptops: Prioritize thermal management during intensive tasks (e.g., CPU/GPU workloads) to prevent temperature-induced capacity fade.
- Wearables: Optimize sensor sampling rates and low-power communication protocols (e.g., Bluetooth Low Energy, BLE) to extend battery life between charges.
- Cross-Device Ecosystems: Implement energy-aware task allocation to offload work to devices with more available battery capacity.

8.4   Conclusion

The proposed electro-thermal model and strategies can extend battery life by 15~30% through a balance of "energy budget" utilization and cumulative drain minimization. Key innovations include a first-principles model ensuring physical consistency, dual-criterion Time to Empty (TTE) prediction, and a scalable framework for multi-device ecosystems. Future work should focus on real-time parameter estimation to enable personalized battery optimization.

References

[1]   Q. Wang, S. Wang, G. Zhou, et al. "Analysis and Research Progress of Lithium Battery Failure". In: *Acta Physica Sinica* 67.12 (2018).

[2]   Z. P. Sun, L. D. Chen, Z. J. Xu, et al. "Analysis of typical temperature and rate discharge char-
      acteristics of Li-ion batteries". In: *Chinese Journal of Power Sources* 44.8 (2020), pp. 1090–
      1092.

[3]   K. S. Ng et al. "Enhanced coulomb counting method for estimating state-of-charge and state-
      of-health of lithium-ion batteries". In: ().

[4]   Q. Huang. "Research on the Thermal Effects and Safety Performance of Lithium-Ion Batter-
      ies". In: (2007).

[5]   OpenAI. *ChatGPT: Optimizing Language Models for Dialogue*. 2024. URL: https://openai.
      com/chatgpt (visited on 01/08/2024).

Appendices

Appendix A   Gillespie algorithm

Algorithm 2 Continuous-time Markov Chain Simulation

 1: Initialize $s(0) = $ Idle, $t = 0$.
 2: **while** $t < T_{\max}$ **do**
 3:      Compute waiting time $\tau \sim \text{Exp}(-Q_{s(t),s(t)})$.
 4:      Select next state j with probability proportional to $Q_{s(t),j}$.
 5:      Update $s(t + \tau) = j$, $t = t + \tau$.
 6: **end while**

Appendix B   Adaptive Battery-Temperature-Aware Power Management Algorithm

This algorithm is a dedicated dynamic power management solution for embedded/edge devices. Based on dual-dimensional data of battery State of Charge (SOC) and real-time device temperature, it dynamically adjusts CPU operating frequency and network bandwidth limits to achieve intelligent balance between performance and power consumption. It effectively solves problems such as insufficient battery life at low power and device lag/damage due to high-temperature operation.

Core Design Concept: Hierarchical Regulation, On-Demand Energy Saving. Divide 3 levels of power strategies according to the threshold ranges of SOC and temperature to avoid sudden performance drop caused by a single energy-saving strategy, and balance device operation efficiency and power consumption control.

Algorithm Regulation Logic Flow

- Real-time Collection: Battery SOC (0~100%) + Device Temperature (°C)
- Threshold Judgment: Match low power/high temperature thresholds to determine power gear
- Parameter Delivery: Set corresponding CPU frequency + network bandwidth limit
- Cyclic Execution: Repeat collection-judgment-delivery process at fixed intervals

```python
import time
from collections import namedtuple
PowerState = namedtuple('PowerState', ['cpu_freq', 'network_limit'])
def read_battery_soc():
    return 75
def read_device_temp():
    return 32
def set_cpu_freq(freq):
    print(f"[Hardware Delivery] Set CPU Operating Frequency $\to$ {freq} MHz")
def set_network_limit(limit):
    print(f"[Hardware Delivery] Set Network Bandwidth Limit $\to$ {limit} Mbps
        ↪ ")
def get_hardware_data():
    soc = read_battery_soc()
    temp = read_device_temp()
    return soc, temp
class PowerManager:
    def __init__(self):
        self.low_soc_threshold = 20
        self.high_temp_threshold = 45
        self.power_gear = {
            'high': (1800, 100),
            'mid': (1200, 50),
            'low': (600, 10)
        }
    def adjust_power(self, soc, temp):
        if temp >= self.high_temp_threshold or soc <= self.low_soc_threshold:
            return PowerState(*self.power_gear['low'])
        elif 30 <= soc < 80 or 35 <= temp < self.high_temp_threshold:
            return PowerState(*self.power_gear['mid'])
        else:
            return PowerState(*self.power_gear['high'])
if __name__ == "__main__":
    pm = PowerManager()
    cycle_limit = 5
    current_cycle = 0
    print(f"Regulation Parameters: Low SOC Threshold {pm.low_soc_threshold}% |
        ↪   High Temperature Threshold {pm.high_temp_threshold}$^{\circ}$C")
    print(f"Cycle Count: {cycle_limit} times | Collection Interval: 1 second\n
        ↪ ")
    while current_cycle < cycle_limit:
        soc, temp = get_hardware_data()
        power_state = pm.adjust_power(soc, temp)
        print(f"[Collection Data] SOC={soc}% | Device Temperature={temp}$^{\
            ↪ circ}$C")
        print(f"[Regulation Result] CPU Frequency={power_state.cpu_freq}MHz |
            ↪ Network Limit={power_state.network_limit}Mbps")
        set_cpu_freq(power_state.cpu_freq)
        set_network_limit(power_state.network_limit)
        time.sleep(1)
        current_cycle += 1
        print("-" * 60 + "\n")
    print(f"Total Execution Times:{current_cycle}|Regulation Logic:Normal")
```

Report on Use of AI

In the context of the COMAP mathematical modeling competition, our team placed strong emphasis on academic integrity and competition fairness. We conscientiously utilized artificial intelligence (AI) tools to enhance our research efficiency, deepen analytical insights, and refine the development of our solutions. Throughout the process, we maintained a responsible approach toward the application of this technology.Accordingly, within this report, we transparently documented each instance of AI usage, demonstrating not only its technical application but also our commitment to ethical considerations. This disclosure was intended to uphold the principles of academic integrity and to reflect our dedication to transparency and accountability in scientific practice.We believe this approach clearly highlighted our team's responsible engagement with AI tools while underscoring our respect for the norms of fair competition.

1. OpenAI ChatGPT [5] (Feb 1, 2024 version, ChatGPT-4)

    Query1: If I want to add the command "nosep" in the cls file, the compilation process using XeTeX will suddenly be interrupted, and there won't be any prompt displayed in the output terminal of VSCode. What's going on?

    We noticed that the enumitem package is typically used to modify the formatting of list environments (such as itemize and enumerate). In the existing code, we already have some settings related to lists, such as using the paralist package. To ensure the correct loading order of the packages and avoid conflicts, we recommend loading the enumitem package after the paralist package, as the paralist package also modifies list environments. However, since we have already used the paralist package and enumitem and paralist may have conflicts, we need to be careful.

    However, in the mcmthesis template, we noticed that the paralist package has already been loaded. The paralist package provides some parallel list environments, while the enumitem package provides more fine-grained control over list environments. Since we only want to set the spacing of the lists, loading the enumitem package and setting the nosep option is reasonable.

    However, to avoid package conflicts, we can use some options when loading enumitem. According to the documentation of enumitem, we can use the shortlabels option to maintain compatibility with paralist. But a safer approach is to load enumitem after paralist and set the appropriate options.

    In addition, we also need to note that the enumitem package may be relied upon by other parts of the document, so it is best to load it after loading all the packages that may modify the list environment.

2. OpenAI ChatGPT (Feb 2, 2024 version, ChatGPT-4)

    Query1: I previously tried methods such as adjusting the loading order of macros, but all of them were ineffective. This indicates that we need a more fundamental solution. Based on the logs and context provided by the compiler, the core of the problem is likely that the hyperref macro package has a deep conflict with specific elements in the document (possibly triggered by the nosep setting of enumitem) when generating PDF bookmarks. What do you think?

Output: Firstly, the user's question is about how to remove the spacing in the itemize list in La-TeX. Looking back at the history, the user attempted to use the nosep option from the enumitem package, but encountered a compilation error, possibly due to a conflict with the hyperref package. The user now asks if there are any alternative solutions. From the conversation history, the user has tried: - Adding the enumitem package and in mcmthesis.cls. - Adjusting the loading order of packages. - Modifying the hyperref settings.

However, the problem persists. The user now wants an alternative solution. My role is a professional document and link handling assistant. I need to answer the question based on the provided document content (i.e., the mcmthesis.cls file) and link content (but the link content is mainly the license and the homepage, not directly relevant) provided. If the document content is insufficient, I can provide suggestions based on pre-trained knowledge. The provided document is the mcmthesis.cls file, which is a LaTeX class file used for MCM/ICM paper templates. The user wants to remove the spacing of the itemize list.

From the content of the provided mcmthesis.cls file, I can see that the paralist package has been loaded . The paralist package provides the compactitem environment, which can create lists without spacing. Therefore, a simple alternative is to use the compactitem environment of the paralist package instead of the standard itemize environment.

3. OpenAI ChatGPT (Feb 2, 2024 version, ChatGPT-4)

Query1: It seems that the root cause of the problem has been identified. If I comment out the macro packages for "algorithm" and "algorithmic" as well as the corresponding pseudo-code, while keeping the "subcaption" package, the compilation can be carried out smoothly. However, there will be warnings when referencing. In the full text, multiple references are made, and specific numbers will be replaced with question marks. If I do not comment out the pseudo-code and "algorithm" and "algorithmic", but instead remove and place the images separately, the compilation can be done smoothly and there will be no errors.

Output: We have identified the root cause of the problem: the algorithm and algorithmic packages, along with the subcaption package, conflict when used simultaneously to display side-by-side images. This might be due to their attempts to modify LaTeX's floating environment or title mechanism, resulting in incompatibility. The solution is as follows:

- Replace algorithm and algorithmic with algorithm2e or algorithmicx packages. However, note that the MCM template already loads algorithm and algorithmic, so we need to comment out these two packages in the cls file and then load the alternative packages in the main document.
- Use minipage or subfig packages to display side-by-side images, but since you have already tried subcaption, we are considering replacing the pseudo-code packages.
- Comment out the loading of algorithm and algorithmic in the cls file, and then load algorithm2e or algpseudocode (the pseudo-code style of algorithmicx) in the main document.